

Time-resolved Scattering of a Single Photon by a Single Atom

Victor Leong,^{1,2} Mathias Alexander Seidler,¹ Matthias Steiner,^{1,2} Alessandro Cerè,¹ and Christian Kurtsiefer^{1,2}



¹Center for Quantum Technologies, 3 Science Drive 2, Singapore 117543

²Department of Physics, National University of Singapore, 2 Science Drive 3, Singapore 117542

(Dated: August 26, 2016)

Scattering of light by matter has been studied extensively in the past. Yet, the most fundamental process, the scattering of a single photon by a single atom, is largely unexplored [1–3]. One prominent prediction of quantum optics is the deterministic absorption of a traveling photon by a single atom, provided the photon waveform matches spatially and temporally the time-reversed version of a spontaneously emitted photon [4–12]. Here, we experimentally address this prediction and investigate the influence of the temporal profile of the photon on the scattering dynamics using a single trapped atom and heralded single photons. In a time-resolved measurement of the atomic excitation we find a 56(11)% increase of the peak excitation by photons with an exponentially rising profile compared to a decaying one. However, the overall scattering probability remains the same within the experimental uncertainties. Our results demonstrate that tailoring the envelope of single photons enables precise control of the photon-atom interaction.

The efficient excitation of atoms by light is a prerequisite for many proposed quantum information protocols. Strong light-matter interaction by using either large ensembles of atoms [13, 14] or single atoms inside cavities [15–17] has received much attention in the past. More recently, significant light-matter interaction has also been observed between single quantum systems and weak coherent fields in free space [18–23]. The time-reversal symmetry of Schroedinger’s and Maxwell’s equations suggests that the conditions for perfect absorption of an incident single photon by a single atom in free space can be found from the reversed process, the spontaneous emission of a photon from an atom prepared in an excited state. There, the excited state population decays exponentially with a time constant given by the radiative lifetime τ_0 of the excited state, and an outward-moving photon with the same temporal decay profile emerges in a spatial field mode corresponding to the atomic dipole transition [24]. Therefore, for efficient atomic excitation the incident photon should have an exponentially rising temporal envelope with a matching time constant τ_0 and propagate in the atomic dipole mode towards the position of the atom [25].

For a more quantitative description of the scattering process we follow Ref. [7], which assumes a stationary two-level atom interacting with a propagating sin-

gle photon in the Weisskopf-Wigner approximation. The photon-atom interaction strength depends on the spatial overlap $\Lambda \in [0, 1]$ of the atomic dipole mode with the propagating mode of the photon, where $\Lambda = 1$ corresponds to complete spatial mode overlap. In this work, we consider scattering of exponentially decaying and rising photons described by the probability amplitude $\xi(t)$

$$\xi_{\downarrow}(t) = \frac{1}{\sqrt{\tau_p}} \Theta(t) e^{-\frac{t}{2\tau_p}} \quad \text{and} \quad \xi_{\uparrow}(t) = \frac{1}{\sqrt{\tau_p}} \Theta(-t) e^{\frac{t}{2\tau_p}}, \quad (1)$$

where $\Theta(t)$ is the Heaviside step function and τ_p is the coherence time of the photon. Integrating the equations of motion in Ref. [7] leads to analytic expressions for the time-dependent population $P_e(t)$ in the excited state of the atom for both photon shapes:

$$P_{e,\downarrow}(t) = \begin{cases} \frac{4\Lambda\tau_0\tau_p}{(\tau_0 - \tau_p)^2} \Theta(t) \left(e^{-\frac{t}{2\tau_0}} - e^{-\frac{t}{2\tau_p}} \right)^2 & \text{for } \tau_p \neq \tau_0 \\ \frac{\Lambda t^2}{\tau_0^2} \Theta(t) e^{-\frac{t}{\tau_0}} & \text{for } \tau_p = \tau_0 \end{cases} \quad (2)$$

and

$$P_{e,\uparrow}(t) = \frac{4\Lambda\tau_0\tau_p}{(\tau_p + \tau_0)^2} \left[e^{\frac{t}{\tau_p}} \Theta(-t) + e^{-\frac{t}{\tau_0}} \Theta(t) \right]. \quad (3)$$

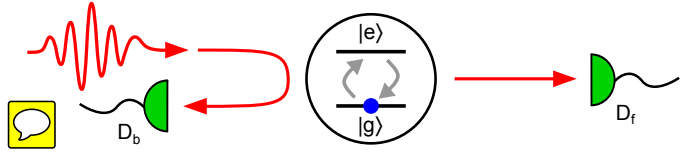


FIG. 1. An incident single photon excites a two-level atom in free-space. The time evolution of the atomic excited state population can be inferred by measuring photons in the forward or backward direction.

In our experiment (Fig. 1) we focus single probe photons onto a single atom, and infer the atomic excited state population $P_e(t)$ from photons arriving at the forward and backward detectors D_f and D_b . We obtain $P_e(t)$ directly from the atomic fluorescence measured at the backward detector D_b with the detection probability per unit time $R_b(t)$,

$$P_e(t) = \frac{\tau_0}{\eta_b} R_b(t) \quad (4)$$

where η_b is the collection efficiency. However, the detection rate in such an experiment is relatively small and

therefore susceptible to detector noise. Alternatively, $P_e(t)$ can be determined from the detection rate at the forward detector D_f with a better signal-to-noise ratio. The probability per unit time of detecting a photon in the forward direction at time t is given by $R_{f,0}(t) = |\xi(t)|^2$ without an atom, and by $R_f(t) = \left| \xi(t) - \sqrt{\frac{\Lambda}{\tau_0}} P_e(t) \right|^2$ with an atom present. The atom alters the rate of transmitted photons via absorption and re-emission towards the forward detector D_f . Therefore, any change $\delta(t)$ of the forward detection rate is directly related to a change of the atomic population,

$$\delta(t) = R_{f,0}(t) - R_f(t). \quad (5)$$

The excited state population $P_e(t)$ is then obtained by integrating a rate equation,

$$\dot{P}_e(t) = \delta(t) - \frac{(1 - \Lambda)}{\tau_0} P_e(t), \quad (6)$$

where the last term describes spontaneous emission into modes that do not overlap with the excitation mode. A schematic of the experimental setup is shown in Fig. 2. A single ^{87}Rb atom is trapped at the joint focus of an aspheric lens pair (numerical aperture 0.55) with a far-off-resonant optical dipole trap (980 nm) [20]. After molasses cooling, the trapped atom is optically pumped into the $5S_{1/2}$, $F=2$, $m_F=-2$ state. Probe photons are prepared by heralding on one photon of a time-correlated photon pair generated via four-wave-mixing (FWM) in a cloud of cold ^{87}Rb atoms [26, 27]. The relevant energy levels are depicted in Fig. 2(b): two pump beams with wavelengths 795 nm and 762 nm excite the atoms from $5S_{1/2}$, $F=2$ to $5D_{3/2}$, $F=3$, and a subsequent ensemble-enhanced cascade decay gives rise to the time ordering necessary for obtaining exponential time envelopes [12, 28, 29]. Dichroic mirrors, interference filters and coupling into single mode fibers select photon pairs of wavelengths 776 nm (herald) and 780 nm (probe). Adjusting the atomic density of the atomic ensemble [27], we set the coherence time $\tau_p = 13.3(1)$ ns of the generated photons, corresponding to a spectral overlap with the atomic linewidth of approximately 90% [30].

To control the temporal envelope of the probe photon, the heralding mode is coupled to a bandwidth-matched, asymmetric Fabry-Perot cavity. The cavity reflects the herald photons with a dispersive phase shift depending on the cavity resonance frequency. Tuning the cavity on resonance or far-off resonance (70 MHz) with respect to the center frequency of the herald photon results in exponentially rising or decaying probe photons [12]. The FWM source alternates between a laser cooling interval of 140 μs , and a photon pair generation interval of 10 μs , during which we register on average 0.054 heralding events on avalanche photodetector (APD) D_h . The probe photons are guided to the single atom by a single mode fiber. The spatial excitation mode is then defined by

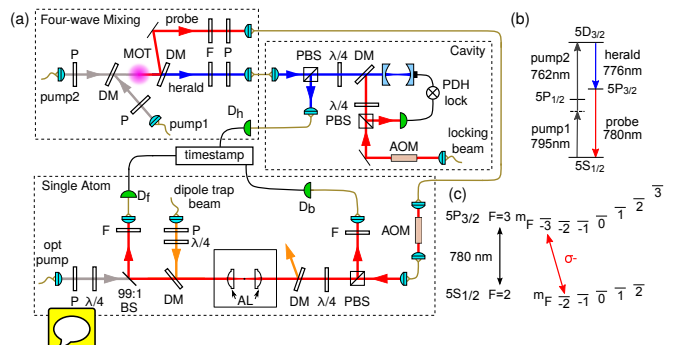


FIG. 2. (a) Experimental setup. (Top left) Four-wave mixing part, providing heralded single photons: Pump 1 (795 nm) and Pump 2 (762 nm) are overlapped in a copropagating geometry inside the cold cloud of ^{87}Rb atoms in a magneto-optical trap, generating pairs of herald (776 nm) and probe (780 nm) photons. The detection of a photon at D_h heralds a probe photon. (Top right) Tuning the resonance of a bandwidth-matched cavity with respect to the heralding photon frequency controls the temporal envelope. (Bottom) Single atom part: A ^{87}Rb atom is trapped at the focus of a confocal aspheric lens pair (AL; numerical aperture 0.55) with a far-off-resonant optical dipole trap (980 nm). The probe photons are guided to the single atom part by a single mode fiber and focused onto the atom by the first AL. Avalanche photodetectors D_f and D_b detect photons collected in forward and backward directions. An acousto-optic modulator (AOM) shifts the probe photon frequency to compensate for the shift of the atomic resonance frequency caused by the bias magnetic field and the dipole trap. D_h , D_f , D_b : avalanche photodetectors (APDs), P: polarizer, F: interference filters, $\lambda/2$, $\lambda/4$: half- and quarter-wave plates, (P)BS: (polarizing) beam splitter, DM: dichroic mirror. (b) Relevant level scheme of the four-wave mixing process in a cloud of ^{87}Rb atoms. (c) Relevant level scheme of the single ^{87}Rb atom in the dipole trap. The probe photons are resonant with the closed transition $|g\rangle = 5S_{1/2}$, $F=2$, $m_F=-2$ to $|e\rangle = 5P_{3/2}$, $F=3$, $m_F=-3$.

the collimation lens at the output of the fiber and the high numerical aperture aspheric lens AL. From the experimental geometry we expect a spatial mode overlap of $\Lambda \approx 0.03$ with the atomic dipole mode [10]. The excitation mode is then collimated by a second aspheric lens, again coupled into a single-mode fiber, and sent to the forward detector D_f . A fraction of the photons scattered by the atom is collected in the backward direction, and similarly fiber-coupled and guided to detector D_b .

To investigate the dynamics of the scattering process, we record photoevent detection times at the forward detector D_f with respect to heralding events at D_h . When no atom is trapped, we obtain the reference histograms $G_{f,0}(t_i)$ for exponentially decaying and rising probe photons, with time bins t_i of width Δt (Fig. 3, black circles). The observed histograms resemble closely the ideal asymmetric exponential envelopes, described by Eq. 1. The total probability of a coincidence event within a time interval of 114 ns ($\approx 8\tau_p$) is $\eta_f = 3.70(1) \cdot 10^{-3}$. When an atom is trapped, we record his-

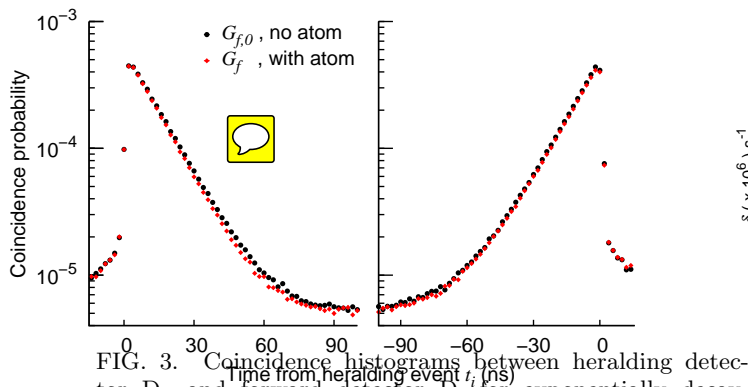


FIG. 3. Coincidence histograms between heralding detector D_h and forward detector D_f for exponentially decaying (left) and rising (right) probe photons with a coherence time $\tau_p = 13.3(1)$ ns obtained from a fit. Black circles: $G_{f,0}$, reference data taken without the trapped atom. Red diamonds: G_f , data taken with the atom present. The time bin size is $\Delta t = 2$ ns. Total measurement time is 1500 hours. Error bars are smaller than the symbol size. We offset all detection times by 879 ns to account for delays introduced by electrical and optical lines.

tograms $G_f(t_i)$ (Fig. 3, red diamonds). The two histograms $G_f(t_i)$ are very similar to the respective reference histograms $G_{f,0}(t_i)$. To reveal the scattering dynamics we obtain the photon detection probabilities per unit time at the forward detector $R_f(t_i) = G_f(t_i)/(\eta_f \Delta t)$ with and without atom in order to use Eq. (5-6) to reconstruct the excited state population $P_e(t_i)$. Figure 4 shows the difference $\delta(t_i) = R_{f,0}(t_i) - R_f(t_i)$ for both photon envelopes, with mostly positive values. A positive value of $\delta(t_i)$ corresponds to net absorption, i.e., a reduction of the number of detected photons during the time bin t_i due to the interaction with the atom. For a photon with a decaying envelope, the absorption is close to zero at $t_i = 0$, and reaches a maximum at $t_i \approx 15$ ns, followed by a slow decay. In strong contrast, the absorption for photons with a rising envelope follows the exponential envelope of the photon, with a maximum absorption rate twice as high as that for photons with a decaying envelope.

We obtain analytical solutions for the expected differences in transmission $\delta(t)$ from Eq. 5 assuming the ideal photon envelopes Eq. (1-2). The magnitude and the dynamics of the observed scattering are well reproduced for $\tau_p = 13.3$ ns and $\Lambda = 0.033$ (Fig. 4, solid lines). The observed peak absorption for the exponentially decaying photon is slightly higher than expected. We attribute this discrepancy to the imperfect photon envelopes which differ slightly from the ideal asymmetric exponential.

The interaction with the atom reduces the overall transmission into the forward detection path for both photon shapes. To quantify this behavior, we calcu-

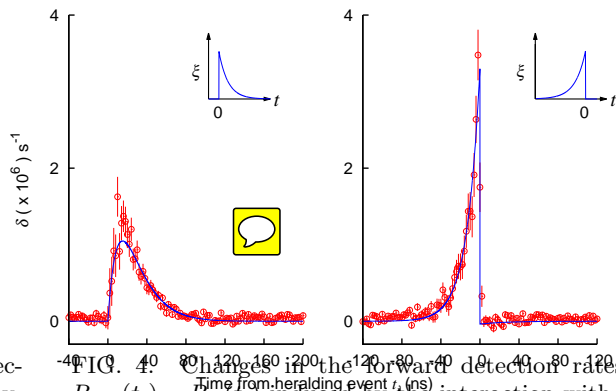


FIG. 4. Changes in the forward detection rates $\delta(t_i) = R_{f,0}(t_i) - R_f(t_i)$ induced by the interaction with the atom. The time bin size is 2 ns. Solid lines: analytical solution of Eq. 5 using Eq. (1,2) for $\tau_p = 13.3$ ns, $\Lambda = 0.033$. Left and right columns show results for exponentially decaying and rising probe photons, respectively.

late the extinction $\epsilon = \Delta t \sum_i \delta(t_i)$ by summing over the interval $-14 \text{ ns} \leq t_i \leq 100 \text{ ns}$ for exponentially decaying photons, and $-100 \text{ ns} \leq t_i \leq 14 \text{ ns}$ for exponentially rising photons, capturing almost the entire photon. We obtain similar extinction values $\epsilon_{\downarrow} = 4.21$ (18)% and $\epsilon_{\uparrow} = 4.40$ (20)% for decaying and rising photons, respectively. The theoretical value of the extinction does not depend on whether the photon envelope is exponentially decaying or rising:

$$\epsilon = \int_{-\infty}^{+\infty} \delta(t) dt = \Lambda (1 - \Lambda) \frac{4\tau_p}{\tau_0 + \tau_p} \quad (7)$$

For our parameters, $\tau_p = 13.3$ ns, $\Lambda = 0.033$, this expression leads to $\epsilon = 4.29\%$, which is close to our experimental results.

The excitation probability $P_e(t_i)$ (Fig. 5, red circles) of the atom is obtained from the differences in the forward detection rates $\delta(t_i)$ and by numerically integrating Eq. (6). The exponentially decaying photon induces a longer lasting but lower atomic excitation compared to the rising photon. We find good agreement with the analytical solutions given in Eq. (2) and (3) (Fig. 5, solid line). We do not observe perfect excitation of the atom from exponentially rising probe photons because of the small spatial mode overlap Λ . However, the peak excited state population for the exponentially rising $P_{e,\text{max},\uparrow} = 2.77$ (12)% is 56(11)% larger than for the decaying one $P_{e,\text{max},\downarrow} = 1.78$ (9)%. The increase in the peak excitation $P_{e,\uparrow,\text{max}}/P_{e,\downarrow,\text{max}} = 78\%$ predicted by Eq. (2) and (3) for $\tau_p = 13.3$ ns, $\Lambda = 0.033$ is also in fair agreement with our findings.

The excited state population can also be directly determined from the atomic fluorescence, Eq. (4). To convert the coincidence histograms $G_b(t_i)$ between the heralding detector D_h and backward detector D_b into the excited

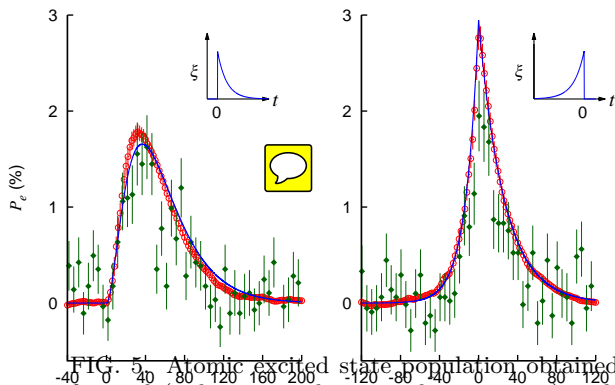


FIG. 5. Atomic excited state population obtained from the forward (red filled diamonds, time bin size 2 ns) and backward detection rates (green filled diamonds, time bin size 5 ns). Solid lines: $P_e(t)$ from Eq. (2) and (3) using $\tau_p = 13.3$ ns, $\Lambda = 0.033$. Left and right columns show results for exponentially decaying and rising probe photons, respectively.

state population $P_e(t_i)$ we have to account for the finite collection and detection efficiencies in the forward and backward path. For the backward path we independently measure the collection efficiency $\eta_b = 0.0126(5)$ and the detector quantum efficiency $\eta_q = 0.56(1)$. Figure 5 (green filled diamonds) shows the inferred excited state population $P_e(t_i) = R_b(t_i)/(\eta_b\Gamma_0) = G_b(t_i)/(\tilde{\eta}_f\eta_q\eta_b\Gamma_0\Delta t)$ with a time bin width of 5 ns, where $\tilde{\eta}_f = 0.0155(4)$ is the heralding efficiency in the forward path, corrected for the collection and detection efficiencies. Again, we find a qualitatively different transient atomic excitation for both photon shapes, in agreement with the theoretical model, but with worse detection statistics compared to the excited state reconstruction using the changes in the forward detection rates. The peak excitation probability and the signal rate can be improved by a larger spatial mode overlap Λ , which is currently limited by the numerical aperture of the focusing lens [31]. Other focusing geometries like parabolic mirrors can theoretically achieve complete mode matching $\Lambda = 1$ [23].

In summary, we have accurately measured the atomic excited state population during photon scattering and have demonstrated that the power spectrum of the incident photon is not enough to fully characterize the interaction. The exponentially rising and decaying photons have an identical Lorentzian power spectrum with a full-width-half-maximum $\Gamma_p = \frac{1}{\tau_p}$, but the transient atomic excitation differs. We have shown that the scattering dynamics depends on the envelope of the photon, in particular that an atom is indeed more efficiently excited by a photon with an exponentially rising temporal envelope compared to an exponentially decaying one. However, when integrated over a long time interval $\Delta t \gg \tau_0, \tau_p$ both photon shapes are equally likely to be scattered as shown by our measurement of the extinction ϵ . The ad-

vantage of exciting single atoms with exponentially rising photons is a larger peak excitation probability within a narrower time interval. Such a synchronization can be beneficial to quantum networks.

Our experimental results also contribute to a long-standing discussion about differences between heralded and “true” single photons [32–35]. The atomic excitation dynamics caused by heralded single photons matches well the one expected from “true” single photon states in our theoretical model, and therefore support a realistic interpretation of photons prepared in a heralding process.

We acknowledge the support of this work by the Ministry of Education in Singapore (AcRF Tier 1) and the National Research Foundation, Prime Minister’s office (partly under grant No. NRF-CRP12-2013-03). M. Steiner acknowledges support by the Lee Kuan Yew Postdoctoral Fellowship.

Methods

Heralded single photon generation: The two pump fields have orthogonal linear polarizations. The 795 nm pump laser is red-detuned by -30 MHz from the $5S_{1/2}, F=2$ to $5P_{1/2}, F=2$ transition to avoid incoherent scattering. The frequency of the 762 nm pump laser is set such that the two-photon transition from $5S_{1/2}, F=2$ to $5D_{3/2}, F=3$ is driven with a blue-detuning of 4 MHz. We can vary the coherence time τ_p of the generated photons by changing the optical density of the atomic ensemble. We choose $\tau_p = 13.3$ ns as a trade-off between matching the excited state lifetime of $\tau_0 = 26.2$ ns and having a high photon pair generation rate. Longer coherence times can be achieved at lower optical densities, but at the cost of lower photon pair generation rates.

The probe photons are guided to the single atom setup by a 230 m long optical fiber. An acousto-optic modulator (AOM) compensates for the 72 MHz shift of the atomic resonance frequency caused by the bias magnetic field (7 Gauss applied along the optical axis) and the dipole trap. The AOM also serves as an optical switch between the two parts of the experimental setup; once a herald photon is detected, the AOM is turned on for 600 ns. The optical and electrical delays are set such that the probe photon passes the AOM within this time interval. Before reaching the atom, the polarization of the probe photons is set to circular σ^- by a polarizing beam splitter and a half-wave-plate.

The Fabry-Pérot cavity used to control the temporal envelope has a length of 125 mm and a finesse of 103(5), resulting in a decay time $\tau_c = 13.6(5)$ ns. The reflectance of the in-coupling mirror and the second mirror are 0.943 and 0.9995 respectively. We use an auxiliary 780 nm laser to stabilize the cavity length using the Pound-Drever-Hall technique.

Data acquisition and analysis: Fig. 3 shows the coincidence histograms without additional processing. For the quantitative analysis (Fig. 4 and Fig. 5) we subtract the accidental coincidence rate from the histograms.

The accidental coincidence rate is caused by background events in the photodetectors, and determined from the histograms by averaging the detected coincidences rate within a 300 ns wide time interval starting about 150 ns after the time interval used to analyze the scattering dynamics.

The total acquisition time for the experiment was 1500 hours, during which the average photon coherence time was $\tau_p = 13.3(1)$ ns and the heralding efficiency was $\eta_f = 3.70(1) \cdot 10^{-3}$. We check for slow drifts in τ_p and η_f by analyzing the histogram $G_{f,0}$ every 60 min for τ_p and 20 min for η_f . The distribution of τ_p is nearly Gaussian with a standard deviation of 0.9 ns, most likely caused by slow drifts of the laser powers and the atomic density; the distribution of η_f has a full-width-half-maximum of $6 \cdot 10^{-4}$. We alternated between the decaying and rising photon profiles every 20 min to ensure that the recorded coincidence histograms are not systematically biased by slow drifts in τ_p and η_f .

Temporal photon envelope: The coincidence histograms recorded without atom (Fig. 3 black circles) differ slightly from the ideal asymmetric exponential functions described in Eq. 1.

These deviations are well explained by the model we use to describe the effect of the cavity [12]. For the exponentially decaying photons, the main deviation is a small rising tail, caused by the finite cavity detuning of 70 MHz. For the exponentially rising photons, we observe a small decaying tail due to the bandwidth mismatch between cavity and photon, and cavity losses.



-
- [1] N. Piro, F. Rohde, C. Schuck, M. Almendros, J. Huwer, J. Ghosh, A. Haase, M. Hennrich, F. Dubin, and J. Eschner, *Nature Physics* **7**, 17 (2010).
- [2] Y. L. A. Rezus, S. G. Walt, R. Lettow, A. Renn, G. Zumofen, S. Götzinger, and V. Sandoghdar, *Phys. Rev. Lett.* **108**, 093601 (2012).
- [3] J. Brito, S. Kucera, P. Eich, P. Müller, and J. Eschner, *Applied Physics B* **122**, 1 (2016).
- [4] S. Quabis, R. Dorn, M. Eberler, O. Glöckl, and G. Leuchs, *Optics Communications* **179**, 1 (2000).
- [5] D. Pinotsi and A. Imamoglu, *Phys. Rev. Lett.* **100**, 093603 (2008).
- [6] M. Stobińska, G. Alber, and G. Leuchs, *EPL (Europhysics Letters)* **86**, 14007 (2009).
- [7] Y. Wang, J. Minář, L. Sheridan, and V. Scarani, *Phys. Rev. A* **83**, 063842 (2011).
- [8] M. Bader, S. Heugel, A. L. Chekhov, M. Sondermann, and G. Leuchs, *New Journal of Physics* **15**, 123008 (2013).
- [9] S. Heugel, A. S. Villar, M. Sondermann, U. Peschel, and G. Leuchs, *Laser Physics* **20**, 100 (2009).
- [10] S. A. Aljunid, G. Maslennikov, Y. Wang, D. H. Lan, V. Scarani, and C. Kurtsiefer, *Phys. Rev. Lett.* **111**, 103001 (2013).
- [11] C. Liu, Y. Sun, L. Zhao, S. Zhang, M. M. T. Loy, and S. Du, *Phys. Rev. Lett.* **113**, 133601 (2014).
- [12] B. Srivathsan, G. K. Gulati, A. Cerè, B. Chng, and C. Kurtsiefer, *Phys. Rev. Lett.* **113**, 163601 (2014).
- [13] K. Hammerer, A. S. Sørensen, and E. S. Polzik, *Rev. Mod. Phys.* **82**, 1041 (2010).
- [14] M. D. Lukin, *Rev. Mod. Phys.* **75**, 457 (2003).
- [15] S. Gleyzes, S. Kuhr, C. Guerlin, J. Bernu, S. Deléglise, U. B. Hoff, M. Brune, J.-M. Raimond, and S. Haroche, *Nature* **446**, 297 (2007).
- [16] T. Wilk, S. C. Webster, A. Kuhn, and G. Rempe, *Science* **317**, 488 (2007).
- [17] A. Stute, B. Casabone, P. Schindler, T. Monz, P. O. Schmidt, B. Brandstätter, T. E. Northup, and R. Blatt, *Nature* **485**, 482 (2012).
- [18] A. N. Vamivakas, M. Atatüre, J. Dreiser, S. T. Yilmaz, A. Badolato, A. K. Swan, B. B. Goldberg, A. Imamoglu, and M. S. Ünlü, *Nano Letters* **7**, 2892 (2007).
- [19] G. Wrigge, I. Gerhardt, J. Hwang, G. Zumofen, and V. Sandoghdar, *Nat Phys* **4**, 60 (2008).
- [20] M. K. Tey, Z. Chen, S. A. Aljunid, B. Chng, F. Huber, G. Maslennikov, and C. Kurtsiefer, *Nature Physics* **4**, 924 (2008).
- [21] L. Slodička, G. Hétet, S. Gerber, M. Hennrich, and R. Blatt, *Phys. Rev. Lett.* **105**, 153604 (2010).
- [22] E. W. Streed, A. Jechow, B. G. Norton, and D. Kielpinski, *Nat Commun* **3**, 933 (2012).
- [23] M. Fischer, M. Bader, R. Maiwald, A. Golla, M. Sondermann, and G. Leuchs, *Applied Physics B* **117**, 797 (2014).
- [24] V. Weisskopf and E. Wigner, *Zeitschr. Phys.* **63**, 54 (1930).
- [25] G. Leuchs and M. Sondermann, *Physica Scripta* **85**, 058101 (2012).
- [26] T. Chanelière, D. N. Matsukevich, and S. D. Jenkins, *Phys. Rev. Lett.* **96**, 093604 (2006).
- [27] B. Srivathsan, G. K. Gulati, B. Chng, G. Maslennikov, D. Matsukevich, and C. Kurtsiefer, *Phys. Rev. Lett.* **111**, 123602 (2013).
- [28] J. D. Franson, *Phys. Rev. A* **45**, 3126 (1992).
- [29] G. K. Gulati, B. Srivathsan, B. Chng, A. Cerè, D. Matsukevich, and C. Kurtsiefer, *Phys. Rev. A* **90**, 033819 (2014).
- [30] V. Leong, S. Kosen, B. Srivathsan, G. K. Gulati, A. Cerè, and C. Kurtsiefer, *Physical Review A* **91**, 063829 (2015).
- [31] M. K. Tey, G. Maslennikov, T. C. H. Liew, S. A. Aljunid, F. Huber, B. Chng, Z. Chen, V. Scarani, and C. Kurtsiefer, *New Journal of Physics* **11**, 043011 (2009).
- [32] W. E. Lamb, *Appl. Phys. B* **60**, 77 (1995).
- [33] S. D. Bartlett, T. Rudolph, and R. W. Spekkens, *Int. J. Quantum Inform.* **04**, 17 (2006).
- [34] J. D. Franson, *Phys. Rev. A* **80**, 032119 (2009).
- [35] M. Bashkansky, I. Vurgaftman, A. C. R. Pipino, and J. Reintjes, *Phys. Rev. A* **90**, 053825 (2014).



